Advances in Colloid and Interface Science 252 (2018) 21–37

Contents lists available at ScienceDirect

Advances in Colloid and Interface Science

journal homepage: www.elsevier.com/locate/cis

Historical perspective

Advances in self-healing materials based on vascular networks with mechanical self-repair characteristics

Min Wook Lee [a,b], Seongpil An [a,c], Sam S. Yoon [c,*], Alexander L. Yarin [a,*]

[a] Department of Mechanical and Industrial Engineering, University of Illinois at Chicago, 842 W. Taylor St., Chicago, IL 60607-7022, USA
[b] Multifunctional Structural Composite Research Center, Institute of Advanced Composites Materials, Korea Institute of Science and Technology, Chudong-ro 92, Bondong-eup, Wanju-gun, Jeollabuk-do 55324, Republic of Korea
[c] School of Mechanical Engineering, Korea University, Seoul 136-713, Republic of Korea

ARTICLE INFO

Available online 24 December 2017

Keywords:
Self-healing
Nanofibers
Mechanical properties
Biomimetic

ABSTRACT

Here, we review the state-of-the-art in the field of engineered self-healing materials. These materials mimic the functionalities of various natural materials found in the human body (e.g., the healing of skin and bones by the vascular system). The fabrication methods used to produce these "vascular-system-like" engineered self-healing materials, such as electrospinning (including co-electrospinning and emulsion spinning) and solution blowing (including coaxial solution blowing and emulsion blowing) are discussed in detail. Further, a few other approaches involving the use of hollow fibers are also described. In addition, various currently used healing materials/agents, such as dicyclopentadiene and Grubbs' catalyst, poly(dimethyl siloxane), and bisphenol-A-based epoxy, are described. We also review the characterization methods employed to verify the physical and chemical aspects of self-healing, that is, the methods used to confirm that the healing agent has been released and that it has resulted in healing, as well as the morphological changes induced in the damaged material by the healing agent. These characterization methods include different visualization and spectroscopy techniques and thermal analysis methods. Special attention is paid to the characterization of the mechanical consequences of self-healing. The effects of self-healing on the mechanical properties such as stiffness and adhesion of the damaged material are evaluated using the tensile test, double cantilever beam test, plane strip test, bending test, and adhesion test (e.g., blister test). Finally, the future direction of the development of these systems is discussed.

Contents

1. Introduction . . . 22
2. Fabrication of vascular nanofiber networks . . . 22
   2.1. Electrospinning . . . 22
      2.1.1. Co-electrospinning . . . 22
      2.1.2. Emulsion spinning . . . 23
   2.2. Solution blowing . . . 23
      2.2.1. Coaxial solution blowing . . . 24
      2.2.2. Emulsion blowing . . . 24
   2.3. Tube and channel networks . . . 24
   2.4. Carbon nanotubes, sacrificial materials, and shape-memory polymers . . . 24
3. Healing materials/agents . . . 25
   3.1. Dicyclopentadiene (DCPD) and Grubbs' catalyst . . . 25
   3.2. Poly(dimethyl siloxane) (PDMS) . . . 26
   3.3. Bisphenol-A-based epoxy . . . 26
4. Characterization of self-healing nanofibers and healing sites and underlying mechanisms . . . 26
   4.1. Visualization . . . 26
   4.2. Spectroscopic characterization . . . 26
   4.3. Thermal analysis . . . 28

* Corresponding authors.
E-mail addresses: skyoon@korea.ac.kr (S.S. Yoon), ayarin@uic.edu (A.L. Yarin).

https://doi.org/10.1016/j.cis.2017.12.010
0001-8686/

5. Evaluation of self-healing . . . 28
5.1. Tensile test . . . 28
5.1.1. Double cantilever beam test . . . 28
5.1.2. Plane strip test . . . 29
5.2. Bending test . . . 29
5.3. Adhesion . . . 29
6. Future directions and concluding remarks . . . 34
Acknowledgement . . . 34
References . . . 35

1. Introduction

Self-healing in nature comprises a fascinating autonomous phenomenon characteristic of most living organisms. For instance, scratched skin and fractured bones are readily healed because of the activation of the human vascular system. The survival of plants, animals, and human beings is facilitated by their ability to recover. However, this characteristic, though highly desirable, is normally absent in engineering materials. The search for bioinspired "self-healing materials" that can self-recover from internal or external damage started in 2001 [1]. In the case of engineered materials, it is desirable that certain embedded healing materials be released at the damaged location (e.g., within internal or external microcracks) and solidify there to stitch/conglutinate the ruptured surfaces in a manner similar to that of blood being delivered by blood capillaries to a wound and triggering the healing process. Nature teaches us that the key element for self-healing is a vascular capillary network that can carry the healing material to the damaged location/wound. Thus, nature-inspired self-healing strategies have been explored in biomimetic engineering designs with the goal of repairing structural damage through the systematic transport of healing materials that can be cured and polymerized at the damaged sites. However, the first approach to the self-healing of engineering materials was far from a natural one, in that it involved the use of discrete embedded microcapsules instead of a vascular capillary network [1]. Fig. 1 illustrates that such capsules are certainly viable and do not require any external energy to trigger the healing process. However, a material layer with such capsules is inherently thick owing to the bulkiness of the microcapsules. Moreover, this approach is inappropriate for repeatable healing, since the capsules can be used only once. Accordingly, a different approach that involves confining the healing materials within smaller structures and allows for repeated healing would be preferable.

In mammals as well as the leaves of plants, vascular networks enable the rapid and continuous transport of healing materials to the damaged location (see Fig. 2). These effective microvascular systems have a network-like structure and cover the entire volume/surface of the body perfectly.

A vascular self-repair system was first demonstrated in [3]. This system was originally proposed for repairing cracks in concrete and restoring its mechanical properties. Subsequently, this approach was expanded to incorporate composite polymeric materials. Healing agents are initially encapsulated within capillaries (e.g., hollow tubes, channels, or electrospun/solution-blown nanofibers). Because the capillaries are interconnected in a network-like structure, one expects that the healing agent will be delivered through this network for multiple local healing events (Fig. 3).

In this review, we describe the recovery characteristics of various vascular-type self-healing engineering materials. The state-of-the-art approaches for fabricating engineering self-healing materials are discussed first. Next, the healing mechanisms involved, including the chemical reactions, are described. After that, examples of self-healing based on the restoration of mechanical properties are discussed. In the concluding section, the scaling-up of the self-healing phenomenon based on the use of nanofibers is discussed from an industrial perspective.

2. Fabrication of vascular nanofiber networks

2.1. Electrospinning

2.1.1. Co-electrospinning

Self-healing agents can be readily encapsulated within core-shell nanofibers formed by coaxial electrospinning [6]. In the first step, which is electrospinning using a coaxial nozzle, the liquid healing

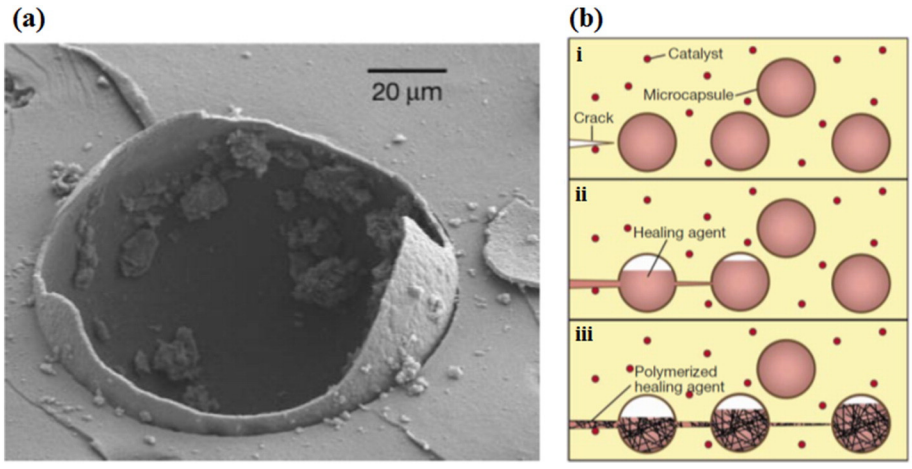

Fig. 1. (a) Scanning electron microscopy (SEM) image showing fracture plane of self-healing material in which ruptured urea formaldehyde microcapsule is embedded in thermosetting matrix. (b) Concept of autonomic healing: healing agent is encased within microcapsules, which are embedded in structural composite matrix containing catalyst capable of polymerizing the healing agent. (i) Cracks form in matrix wherever damage occurs. (ii) Sketch of crack, which ruptures microcapsules, releasing healing agent into crack plane. (iii) Healing agent comes in contact with catalyst dispersed within matrix, which triggers polymerization, resulting in closing of crack faces. Reprinted with permission from [1].

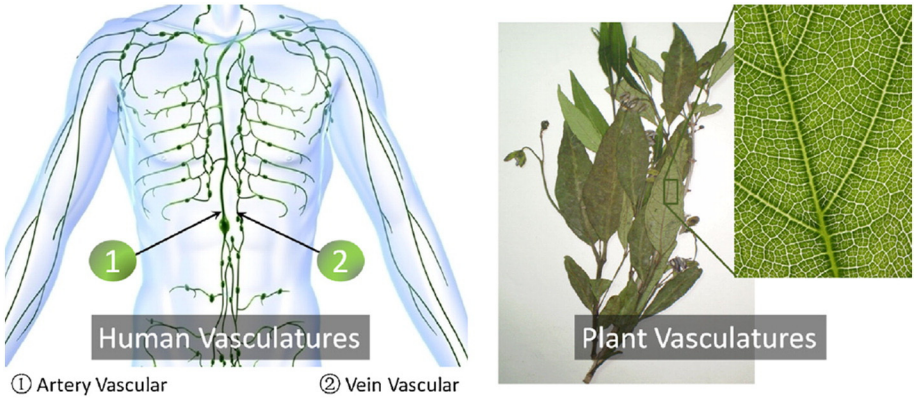

Fig. 2. Branching vasculature networks in animal (or human) body and plant leaves. Reprinted with permission from [2].

agent is supplied through the inner needle and electrospun as the core material inside the shell material [e.g., polyacrylonitrile (PAN) and poly(vinylpyrrolidone) (PVP)], which is supplied by the coaxial needle (see Fig. 4a) [7–12]. Coaxial electrospinning (or co-electrospinning) is a simple and reliable technique for encasing liquid healing agents within continuous nano/microfibers [13]. For example, a resin monomer and curing agent were encapsulated in beaded fibers with a size of 2–10 μm (cross-sectional diameter) [14]. These fibers were significantly smaller than microcapsules, whose dimensions are on the order of $10–10^2$ μm. It is desirable to form thin and uniform fibers for encapsulating the healing agent. In [7,8], bead-free core-shell nanofibers a few hundred nanometers in size were co-electrospun. This approach only requires that the shell material be a spinnable viscoelastic polymer. On the other hand, the core material, that is, the healing agent, does not have to be spinnable (e.g., liquid epoxies). Several types of modifications are possible. For instance, trilayered electrospun nanofibers have been formed using a needle, which supplied three solutions (through the coaxial outer/middle/inner channels) simultaneously [15–18] (see Fig. 4b). In another novel architecture of multiwalled fibers, the healing agent is encapsulated within the core, while the catalyst particles being embedded in the outer layer of the fiber. It is imperative that both components of the healing agent, namely, the resin monomer and catalyst, be present in the crack area, as only this guarantees polymerization and thus healing [19,20].

2.1.2. Emulsion spinning

Emulsion spinning is another approach used to form core-shell nanofibers [21]. In this case, a coaxial needle is not necessary, and a simple single-exit needle is used instead. The method is more convenient than co-electrospinning, as it is easier to control the single-solution jet issuing from the single needle rather than the two-solution jets simultaneously being issued in contact from a co-axial needle. In this case, it is necessary that the core material is emulsified within the polymeric solution that will form the shell (Fig. 5). Thus, instead of a uniform solution, an emulsion is issued from the single needle, with drops of the core material being encapsulated by the surrounding polymeric matrix. As a result, the drops entrapped at the entrance to the Taylor cone are stretched into a core and encased within the shell polymer, where they exhibit electrically driven bending instability and form core-shell fibers [6]. To form self-healing nanofibers, poly(dimethyl siloxane) (PDMS) resin monomer (containing Pt as catalyst) and the curing agent are mixed with n-hexane and emulsified in a PAN/dimethylformamide (DMF) solution (see Fig. 5). The core-shell fibers formed by the emulsion electrospinning process can be used as self-healing nanofibers to facilitate the recovery of bending stiffness as well as to accord corrosion protection [5,8].

2.2. Solution blowing

When a slowly moving polymer jet is emitted coaxially into a high-speed (~150 m/s) jet of air, the stretching caused by drag and the aerodynamically driven bending instability transform the polymer jet into monolithic nanofibers, which dry during their flight in air [6]. A core-shell polymer jet issued from a coaxial needle into a coaxial high-speed air stream undergoes a similar transformation into core-shell nanofibers. In this case, the shell polymers used in electrospinning, such as PAN, nylon-6, and poly(vinylidene difluoride) (PVDF), can be used [22–24]. Solution blowing is more effective for forming core-shell fiber mats than is electrospinning. It was found [24], that the core-to-shell mass ratio for the nanofibers produced by solution blowing is 33 times higher (75.62%) and the total mass production rate is 2 times higher (1.524 g/h) than those for the nanofibers produced by

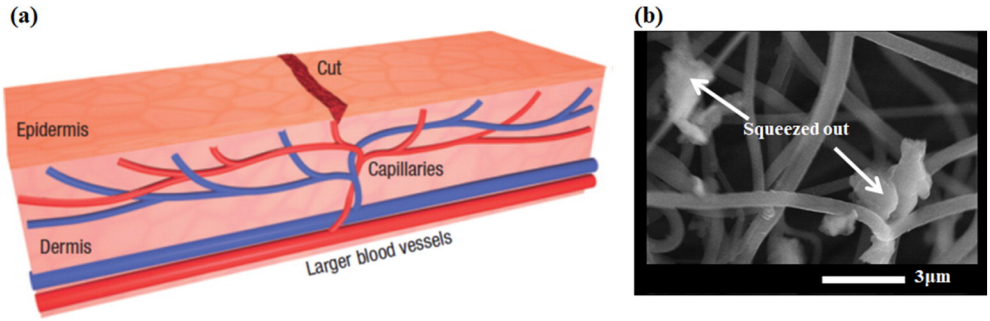

Fig. 3. (a) Schematic diagram of capillary network in dermis layer of skin with cut in epidermis layer. Reprinted with permission from [4]. (b) SEM image of self-healing nanofibers and squeezed-out core (healing) material. Reprinted with permission from [5].

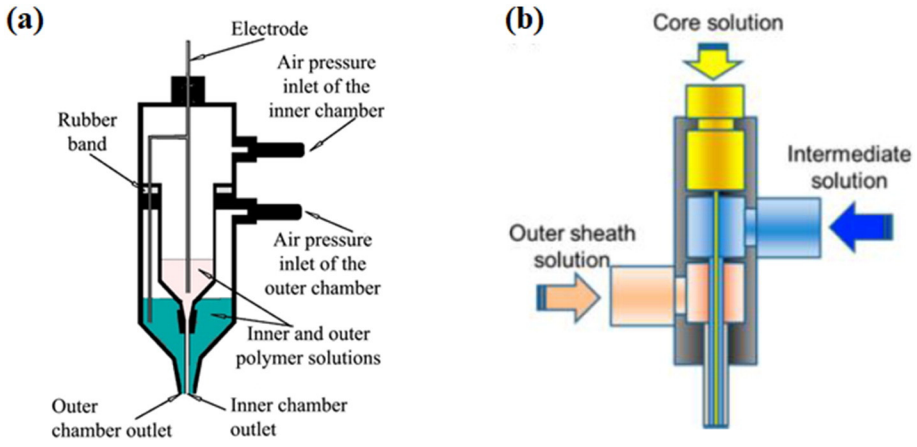

Fig. 4. Experimental setup used for (a) co-electrospinning of core-shell nanofibers. Reprinted with permission from [13]. (b) Triaxial electrospinning. Reprinted with permission from [16].

electrospinning (2.29% and 0.767 g/h, respectively) (see Fig. 6). Further, the mass production rate of monolithic nanofibers (e.g., nylon-6 nanofibers) in the case of solution blowing (10 mL/h) is 33.3 times higher than for electrospinning (0.3 mL/h). Solution-blown self-healing fiber mats contain a significant amount of the healing agent. The greater the amount of the healing agent within the fibers, the greater the chance that the healing agent will be released at the damaged location and heal the damage.

2.2.1. Coaxial solution blowing

Lee et al. [24] reported core-shell microfibers formed by coaxial solution blowing. In these nanofibers either a binary epoxy resin or its hardener was encapsulated within the core, while PVDF was used as the shell material (see Fig. 7). The shell diameter was 0.2–2.6 μm. It should be emphasized that coaxial solution blowing is at least 10 times faster than electrospinning. Thus, solution blowing is one of the most viable processes for the mass production of core-shell nanofibers as it has already been scaled to the industrial level [25]. The larger the fiber diameter, the faster is release of the epoxy resin and its hardener from the fiber cores; this shortens the solidification time as compared to that for electrospun nanofibers.

2.2.2. Emulsion blowing

Sinha-Ray et al. [8] had successfully employed solution blowing to fabricate core-shell fibers from emulsions. Similar to emulsion electrospinning, solution blowing has several advantages. For instance, the manufacturing setup involved is simple and flow control is easy. In the case of emulsion blowing, the core and shell of a slowly moving coaxial jet are entrained by a fast surrounding coaxial air jet. The formed core-shell jet subsequently undergoes stretching and exhibits aerodynamically driven bending instability. Also the solvent evaporates and dry core-shell nanofibers are formed in-flight.

2.3. Tube and channel networks

Fiber-reinforced composites (FRCs) consist of hollow fibers embedded in a surrounding matrix. The first vascular-type composites were fabricated by Bleay et al. [26]. Hollow glass fibers were incorporated within composite panels and then impregnated with an epoxy by a vacuum-assisted capillary-action-based filling technique. The hollow glass fibers, which had diameters in the $10–10^2$ μm range, were used as empty channels in composite laminates, which were subsequently filled with a healing agent (see Fig. 8) [27–29]. On a larger scale, polyvinylchloride (PVC) tubing (inner/outer diameters = 1.5/2.5 mm) was incorporated in sandwich panels in [30]. Further, empty channels to be filled with resin and hardener were prepared by manually pulling out embedded wires ($d = 0.9$ mm) from a sandwich composite once an epoxy layer had been cured in the mold [31].

2.4. Carbon nanotubes, sacrificial materials, and shape-memory polymers

Several other ideas for the fabrication of vascular-like containers for healing agents have been proposed and demonstrated. For example, self-healing materials have been encapsulated within core-shell nanofibers as well as carbon nanotubes (CNTs). A self-healing material was encapsulated within CNTs through self-sustained diffusion [8]. A transmission electron microscopy (TEM) image of a CNT containing a self-healing material is shown in Fig. 9.

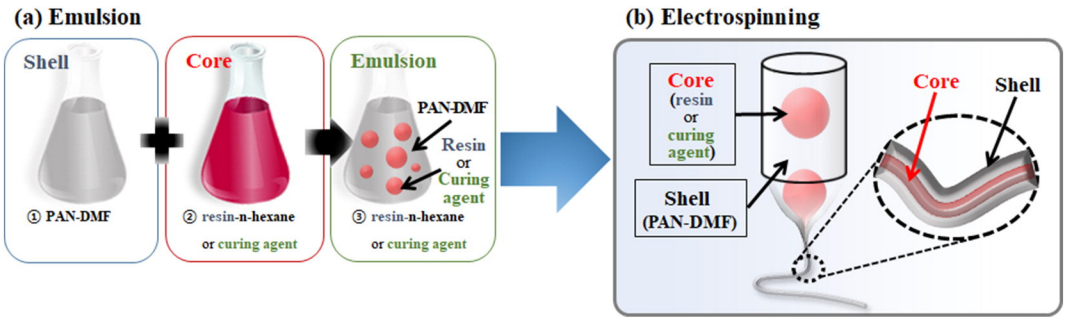

Fig. 5. Schematic showing (a) preparation of shell polymer solution, two core solutions, and two corresponding emulsions. (b) Emulsion electrospinning. Reprinted with permission from [5].

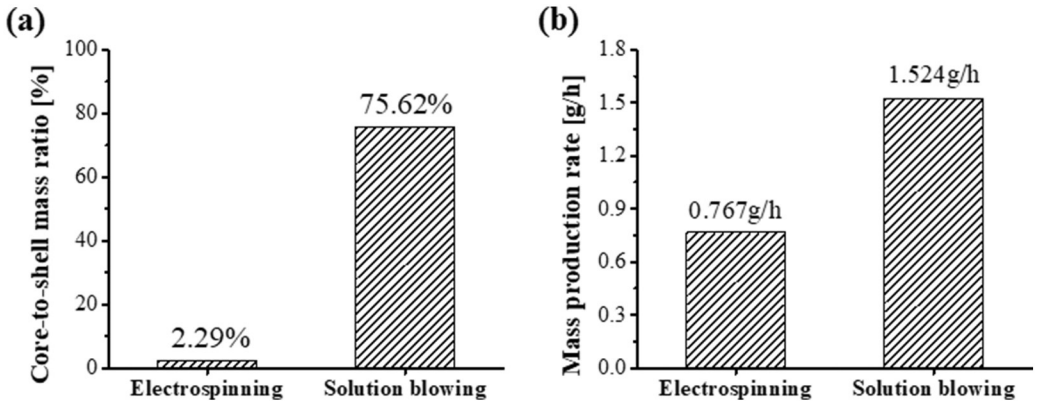

Fig. 6. Comparison of (a) core-to-shell mass ratio and (b) mass production rate of core-shell nano/microfibers produced by coaxial electrospinning and solution blowing. Core and shell materials of electrospun fibers are PDMS resin and PAN while those of solution-blown fibers are epoxy resin and PVDF/polyethylene oxide (PEO). Reprinted with permission from [24].

Three-dimensional vascular networks can be formed in composites by removing a sacrificial material. A pattern of filaments was formed using fugitive ink, which was subsequently melted from the matrix material (see Fig. 10) [31]. Similarly, poly(lactic acid) (PLA) monofilaments (300 μm in diameter) were used as a sacrificial material in a matrix (see Fig. 10) [32]. In these cases, as the sacrificial filaments are removed from the composite by evaporation or melting, the empty channels are infiltrated by the healing material.

Healing agents have also been encapsulated in electrospun fiber mats by immersing the fibers in a liquid epoxy solution [33]. The healing materials were contained in the fiber mats, which were encapsulated within the composite, as shown in Fig. 11.

Shape-memory polymer (SMP)-based materials can also be used for the self-healing of emerging macrocracks [34–38]. An artificial polymer muscle based on a healing-on-demand composite made of a thermoset host, commercial fishing line, and thermoplastic particles has been demonstrated [39]. This artificial muscle is thermally sensitive and contracts when heated; this allows it to pull parts of a cracked material together. The crack-healing process proceeds via the following stages (see Fig. 12) [39]: (i) the polymer composite sample to be healed is reinforced by the polymer artificial muscle and the thermoplastic particles (melting temperature of 58–60 °C) in the matrix; (ii) a crack is initiated by an external load during use; (iii) the crack is closed by the thermal contraction of the artificial muscle (fishing line coil) and healed by the melted particles, which fill the crack under external heating at T = 79 °C; and (iv) after cooling, the crack is filled and cured by the thermoplastic particles, resulting in the re-establishment of continuity between the healing agent and the matrix.

3. Healing materials/agents

3.1. Dicyclopentadiene (DCPD) and Grubbs' catalyst

Dicyclopentadiene (DCPD, $C_{10}H_{12}$) monomer has been used in a number of studies on self-healing, beginning with the original system reported by White et al. [1,7,8,29,40,41]. Ring-opening metathesis polymerization (ROMP) is activated as the DCPD monomer comes in contact with the solid-phase Grubbs' catalyst dispersed within the epoxy matrix (see Fig. 13). The DCPD monomer is highly stable, exhibits low viscosity, and is insensitive to the presence of oxygen and water/humidity under the polymerization conditions [42]. In addition, poly(dicyclopentadiene) (PDCPD) is a highly cross-linkable polymer that exhibits desirable mechanical properties, namely, high toughness and strength [43,44].

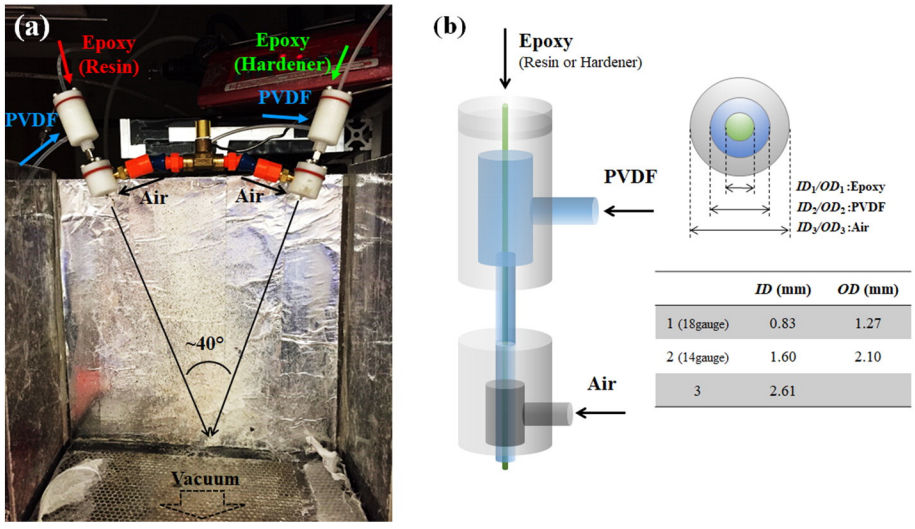

Fig. 7. Solution blowing of core-shell nano/microfibers: (a) experimental setup; (b) design of core-shell needle with coaxial air-blowing nozzle. Epoxy- and hardener-core fibers are produced simultaneously and mixed uniformly in deposited fiber mat. Reprinted with permission from [24].

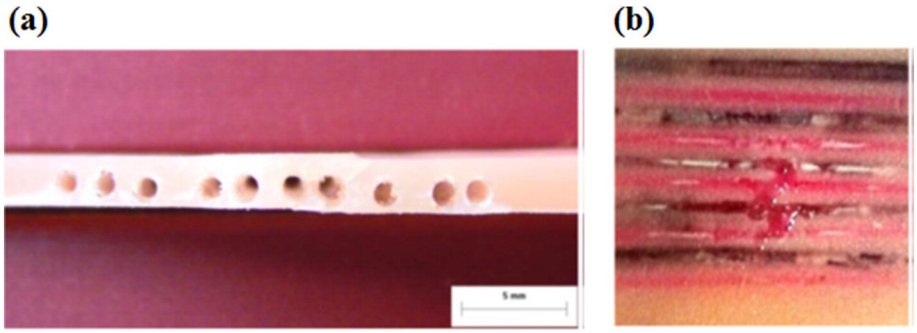

Fig. 8. (a) Cross-section of sample with empty glass tubes. (b) Sample immediately after impact test; liquid self-healing agent released on the surface can be seen. Reprinted with permission from [29].

3.2. Poly(dimethyl siloxane) (PDMS)

PDMS is the cross-linked product of dimethyl siloxane (DMS, resin) and dimethyl-methyl hydrogen-siloxane (curing agent). The chemical structure and curing process of PDMS are briefly explained in Fig. 14. The resin is made of dimethylvinyl-terminated dimethyl siloxane (CAS: 68083-19-2), while the curing agent consists of dimethyl-methyl hydrogen-siloxane (CAS: 68037-59-2). This silicone elastomer shows superior mechanical strength/elasticity, desirable high chemical properties, and good biocompatibility and is thus used widely in microfluidic devices, medical applications, cosmetics, and food items (as an antifoaming agent). The PDMS elastomer was first used for self-healing in [45,46]. The two components of PDMS, namely, the resin and the cross-linker (curing agent), were encapsulated within urethane microcapsules. The encapsulation of PDMS within co-electrospun beaded fibers has also been reported [14]. Furthermore, PDMS has been employed in self-healing composites reinforced with nano/microfibers [5,9–12,47,48]. The two components of PDMS were encased separately within the cores of the core-shell (PAN shell) fibers by means of emulsion spinning or co-electrospinning. This dual self-healing system comprising PDMS resin and curing-agent-encapsulating fibers was subsequently used as a self-healing material [49].

3.3. Bisphenol-A-based epoxy

From a material properties viewpoint, PDMS is one of the most attractive self-healing agents owing to its aforementioned advantages. However, it normally takes 24–48 h to cure fully at room temperature. Further, cured PDMS is soft and flexible. Accordingly, PDMS is not a suitable material for many applications, and other self-healing materials with a shorter curing time and higher strength or stiffness are desirable. Because of this reason, the diglycidyl ether of bisphenol A (DGEBA, $C_{21}H_{24}O_4$), which comprises epichlorohydrin and bisphenol A (BPA, $C_{15}H_{16}O_2$) [51] and constitutes almost 90% of the global epoxy resin market [52], has been used as a healing agent in a number of studies [32,33,49,53–57]. The likely reaction mechanism of DGEBA and diethylenetriamine (DETA) is illustrated in Fig. 15. However, BPA is also being gradually replaced with green materials because of its toxicity and public health concerns [58]. In several studies [24,59,60] a BPA-based commercial epoxy was employed as a healing agent embedded within solution-blown fibers. The epoxy used [24,59,60] set in 5 min and cured fully within 1 h.

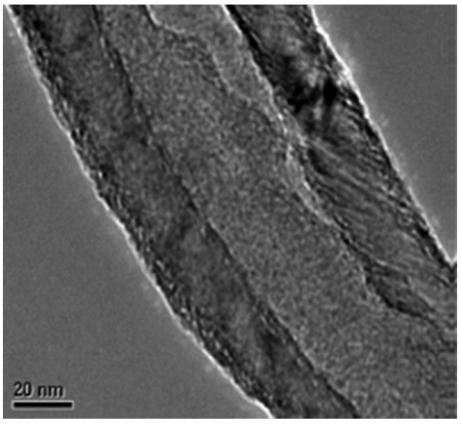

Fig. 9. TEM image of self-healing material (isophorone diisocyanate) encapsulated within CNT. Reprinted with permission from [8].

4. Characterization of self-healing nanofibers and healing sites and underlying mechanisms

4.1. Visualization

To begin with, in order to ensure that the healing materials are encapsulated effectively, defect-free and beads- or blobs-free uniform fibers are preferred. The overall morphology of the fibers containing the self-healing agent can be inspected using optical microscopy [62], scanning electron microscopy (SEM) [63], atomic-force microscopy (AFM) [64], and scanning profilometry [65]. However, only the exterior features can be observed by these methods. The core-shell configuration is one of the most important structural features of self-healing fibers. Thus, the presence of a core filled with the healing agent has to be confirmed using transmission electron microscopy (TEM), which allows for imaging through sufficiently thin shells [11]. Fluorescence imaging is another way to elucidate the encased core material if a fluorescent dye is blended with it [66–68]. The internal damage incurred within a composite can be investigated using ultrasonic C-scanning or X-radiography [26,67,68]. Nanofiber images obtained using the methods described in this subsection are shown in Fig. 16.

4.2. Spectroscopic characterization

The elemental composition of the released healing material can be analyzed using energy-dispersive X-ray spectroscopy (EDX). For example, the presence of PDMS (C_2H_6OSi) embedded in PAN (C_3H_3N) nanofibers has been confirmed by EDX analysis. The spectrum contained a distinct peak related to Si at a K_α value of ~1.8 keV (see Fig. 17) [9,47]. In the case of DCPD ($C_{10}H_{12}$), the EDX spectrum was barely distinguishable from those of most polymer shell materials, which are also generally composed of C and H [8].

Fourier-transform infrared (FTIR) and Raman spectroscopies performed at room temperature in open air can also be used as nondestructive imaging techniques. The healing process, that is, the

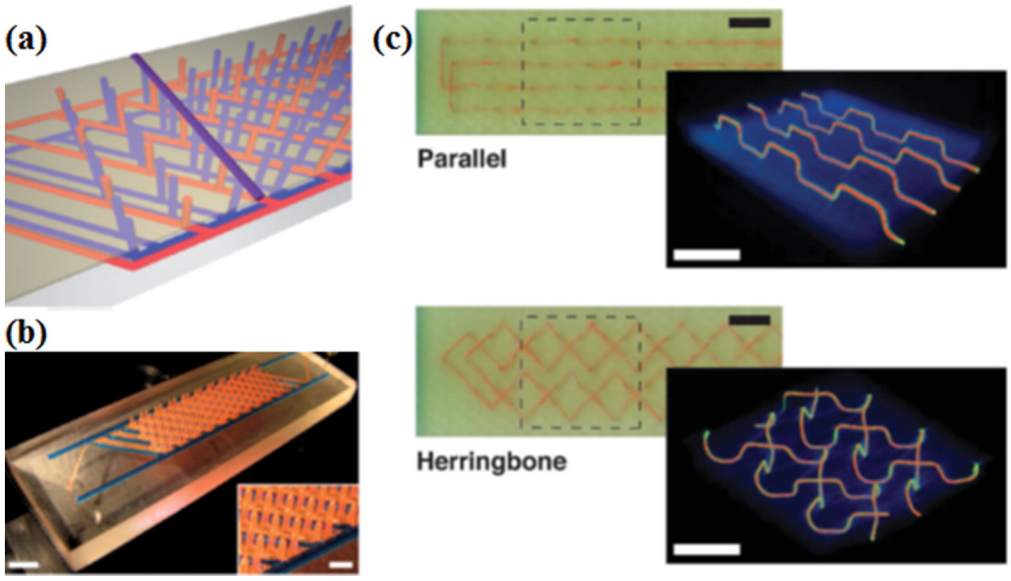

Fig. 10. (a) Schematic view of interpenetrating microvascular network that supplies two fluids (red and blue) to crack plane, where mixing occurs (purple, at lower borderline). Reprinted with permission from [31]. (b) Interpenetrating microvascular network fabricated by direct-write assembly of wax (orange)- and Pluronic (blue)-based fugitive inks. Scale bar is 5 mm. Inset: magnified view of vertically oriented features printed using wax-based ink. Scale bar is 1 mm. Reprinted with permission from [31]. (c) Pre-vascularized, fiber-reinforced composite laminate samples showing sacrificial PLA stitching patterns (scale bars are 10 mm) and post-vascularized, X-ray computed microtomographic reconstructions of vascular networks filled with eutectic gallium indium alloy for radiocontrast. Scale bars are 5 mm. Reprinted with permission from [32].

polymerization of the released healing materials, can be investigated using these techniques [19,20,29]. For example, in the case of DCPD, the bands at wavenumbers of 1572 and 1614 cm^{-1} could be assigned to the ν(C═C) stretching vibrations of the DCPD monomer (see Fig. 18). That the healing process had occurred was confirmed by the fact that the peak at 1572 cm^{-1} disappeared and that at 1614 cm^{-1} underwent a red-shift, suggesting that DCPD has been polymerized [29]. FTIR analysis has also been used to confirm the encapsulation of the hardener and epoxy within the fiber structure. Fig. 18c and d show the FTIR spectra of the hardener and resin, respectively. The peak at 1592 cm^{-1} corresponds to the N—H bending vibrations while the strong peak at 1150 cm^{-1} is related to the stretching of the C—N bond, confirming the presence of the amine-based hardener in the fiber structure (panel c). Further, the peaks at 815 cm^{-1} and 840 cm^{-1}, which belong to the oxirane groups, verify the presence of the epoxy resin within the triaxial fiber structure (panel d) [19].

Raman spectroscopy is another method used to determine the chemical composition of the healed (or unhealed) regions at various locations. The Raman spectrum of PDMS contains peaks related to the Si—O—Si, Si—C, and CH_3 bonds associated with the cured PDMS molecule at wavenumbers of 492, 618/712, and 1265 cm^{-1}, respectively (see Fig. 19) [69]. Spectral peaks related to the uncured resin and the curing agent appear at 1541 and 2168 cm^{-1}, respectively; these correspond to the CH_2—NH—CH_2 and Si—H bonds, respectively, and disappear as the resin and curing agent are polymerized [70]. The presence of these peaks confirms that the resin and curing agent have been released and that the resin has been cured on the PDMS surface. It was found that the resin and curing agent are released/mixed/cured to form extra PDMS chunks that help heal the crack bank [71]. In addition, the self-healing of a BPA-based epoxy resin was also studied using Raman spectroscopy [32]. The resin and hardener exhibited peaks at 1256 cm^{-1} (oxirane ring)/1610 cm^{-1} (phenyl ring) and 1656 cm^{-1} (amide-I), respectively (data not shown here) [61,72,73]. Thus, based on the Raman spectrum of the fracture surface, the delivery of the healing agent as well as the occurrence of the healing (mixing and polymerization) processes was confirmed.

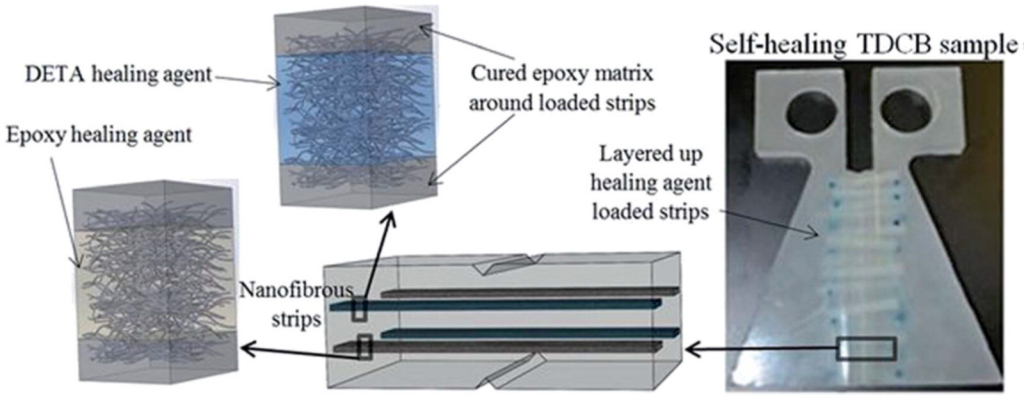

Fig. 11. Schematic of preparation method and resulting structure of self-healing specimen produced using electrospun membrane. Reprinted with permission from [33].

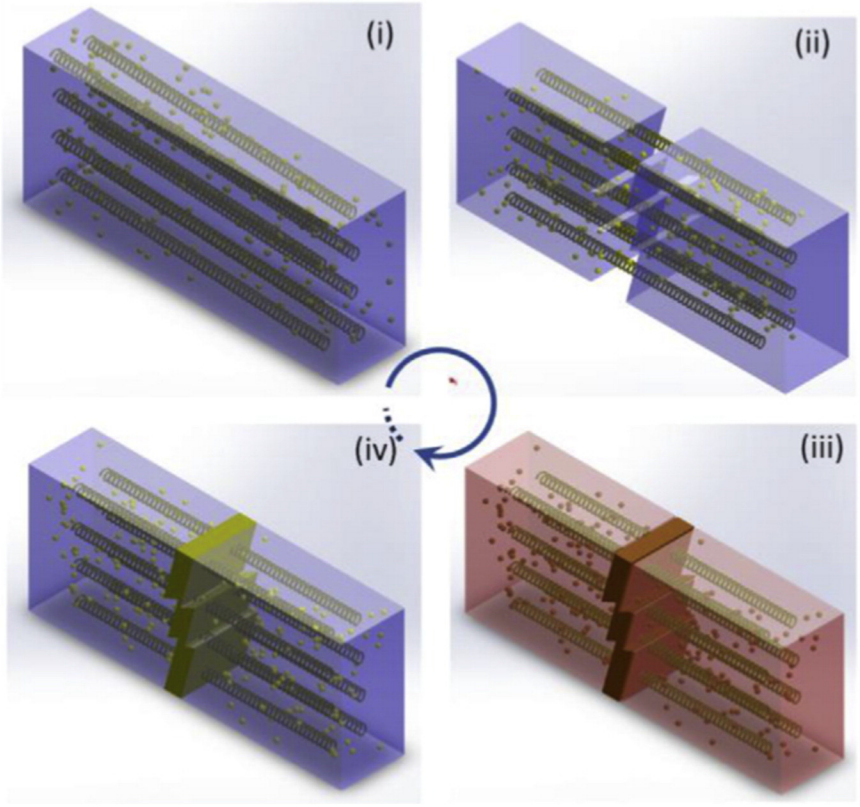

Fig. 12. Schematic of on-demand healing process. Reprinted with permission from [39].

4.3. Thermal analysis

Thermogravimetric analysis (TGA) and differential thermogravimetry (DTG) are useful for confirming that the self-healing cores are encased within the nanofiber shells. Using these thermal analysis methods, the phase-change temperature can be determined (e.g., the melting or evaporation point). The change in the weight owing to the release of a substantial amount of volatile substances or gasification during the phase-change process can be determined through TGA. The DTG is the first derivative of the weight loss curve as observed during TGA and is indicative of the temperatures corresponding to the phase changes. According to previous studies [5,11,47], the evaporation temperature of PDMS resin and its curing agent (uncured) are 576.3 °C (●) and 176.1 °C (♦), respectively, while that of PAN (the shell material) is 305.0 °C (■) (see Fig. 20).

5. Evaluation of self-healing

The mechanical recovery of damaged materials following the self-healing process can manifest itself via changes in the tensile strength, Young's modulus (stiffness), and flexural stiffness. These characteristics can be assessed through the following tests.

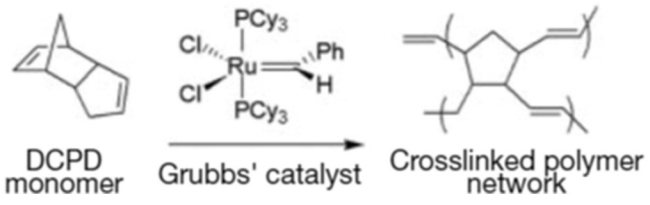

Fig. 13. Polymerization activated by DCPD/Grubbs' catalyst. Reprinted with permission from [1].

5.1. Tensile test

5.1.1. Double cantilever beam test

The double cantilever beam test introduced in [74] has been used widely for evaluating the self-healing characteristics of materials (see Fig. 21) [1,33,40,75–83]. The healing agent employed in the tapered double-cantilever beam (TDCB) specimens filled an open delamination crack and cured it. The load-displacement data were recorded using the delamination crack induced during a mode-I fracture test. The crack-healing efficiency was evaluated through fracture toughness tests performed on virgin and healed specimens. After the first fracture, the specimen was left to provide time for the crack to heal (autonomously). Thus, the ratio of the fracture toughness of the healed specimen ($K_{IC,healed}$) to that of the corresponding virgin one ($K_{IC,virgin}$) was defined as the healing efficiency, η. The crack-length-independent fracture toughness $K_{IC} = \alpha P_C$, where α is a geometric factor determined experimentally [84] and P_C is the critical fracture load. Thus, the quantitative healing efficiency was calculated as follows:

$$\eta = \frac{K_{IC,healed}}{K_{IC,virgin}} = \frac{P_{C,healed}}{P_{C,virgin}} \quad (1)$$

Similarly, the self-healing efficiency of TDCB specimens embedded with epoxy-carrying fiber strips was investigated in [33]. The samples healed at room temperature demonstrated the ability to autonomously recover under the critical fracture load during six repeated tests when neopentyl glycol diglycidyl ether (NGDGE) and diethylenetriamine (DETA) were used.

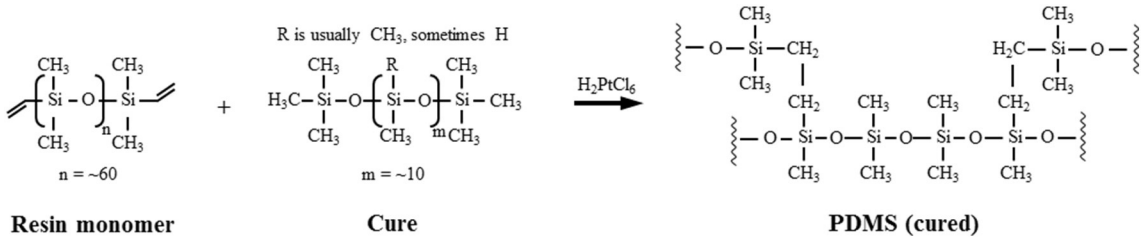

Fig. 14. Chemical structure and curing process of PDMS. Reprinted with permission from [50].

5.1.2. Plane strip test

Tensile tests were performed on electrospun and solution-blown nanofiber mats in order to investigate the stress-strain dependence [6,85–88]. To evaluate the self-healing efficiency of the core-shell electrospun and solution-blown nanofiber mats, their tensile properties were measured before and after damage caused by stretching. Thin self-healing nanofiber mats and fiber-reinforced composite (FRC) specimens shaped as strips were clamped and pulled by pneumatic upper/lower grips at a constant strain rate. Uniaxial stretching tests were conducted under various conditions. For example, (i) a dynamic tensile test was performed at a fixed stretching rate until the sample had ruptured completely [12]; (ii) a dynamic tensile test similar to that in (i) was performed; however, the stretching/releasing process was performed repeatedly [9]; (iii) an interrupted tensile test during which stretching was paused in the middle was also performed [60]; and (iv) a long-duration static fatigue test was performed during which the strain was kept constant [59].

The mechanical characteristics of individual fibrous specimens as well as those of composite fillers deteriorate at a certain level of stretching. However, samples with self-healing core-shell nanofibers exhibited the recovery of accumulating microcracks owing to the healing agents released from the fiber cores. Thus, the self-healing efficiency can be evaluated based on the recovery of the ultimate strength or stiffness as determined from the stress-strain curves (see Fig. 22). Self-healing is also manifested by the arrest of the growth of prenotched cracks [59,71], as also shown in Fig. 22.

5.2. Bending test

The three- and four-point bending tests are classical methods for measuring the stiffness of a material using specimens shaped as a beam (ASTM D790, D6272) [89–93]. They are also suitable for testing multi-ply sandwich-like composite laminates containing a relatively hard epoxy (rigid material) [94–96]. The test specimen has a uniform rectangular cross-section. In the three-point bending test, the specimen is supported by two anvils, and a load is applied at the center between the two supports. The elastic modulus, E_B is calculated using Eq. (2), which involves the measured yield load, L, and the corresponding measured deflection, δ:

$$E_B = \frac{mL^3}{4bd^3} \tag{2}$$

where E_B is the elastic modulus under bending, L is the support span, b is the beam width, d is the beam depth, and m is the slope of the load-deflection curve corresponding to the early linear elastic region ($m = \Delta P/\Delta\delta$).

The recovery ratio, η, is evaluated based on the two flexural strengths and the stiffnesses measured in the corresponding pre- and post-damage tests, respectively [7,8,19,20,27,28,30,53]:

$$\eta = \frac{E_{B,healed}}{E_{B,initial}} \tag{3}$$

According to [7], the flexural stiffness of self-healing PMC (polymer-matrix composite) specimens decreased to 30–50% of the initial pre-damage value and then recovered to 70–100% of the initial value owing to self-healing (Fig. 23a) [7]. In [28], test specimens were damaged by bending but recovered their maximum stiffness almost completely, with the self-healing efficiency being approximately 97% (not shown here). Similarly, Wu et al. demonstrated the self-healing of fractured and delaminated multi-ply PMCs in 2013 (see panel b).

5.3. Adhesion

Since adhesives are also subjected to rupture and failure, self-healing adhesives (e.g., BPA epoxies) are an attractive alternative to conventional ones. In the case of self-healing adhesives, the released healing agent must adhere to the base substrate. The blister test has been employed

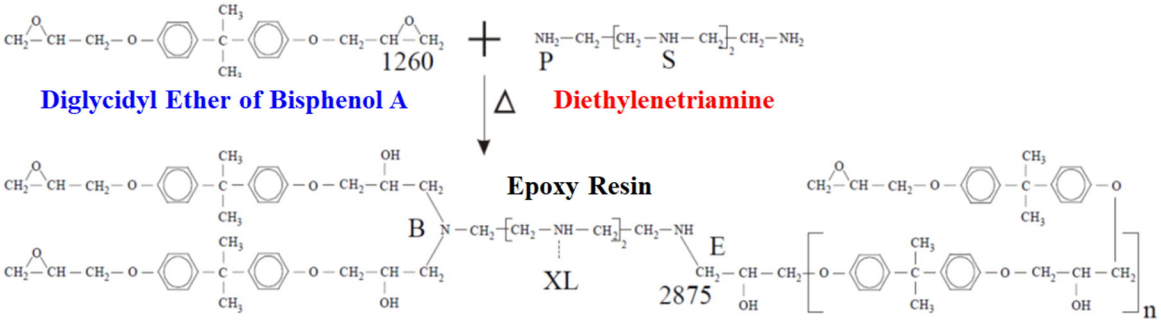

Fig. 15. Chemical structures of DGEBA and DETA and corresponding curing reaction. P is primary amine, E indicates chain extension, B indicates branching, and XL indicates cross-linking. Reprinted with permission from [61].

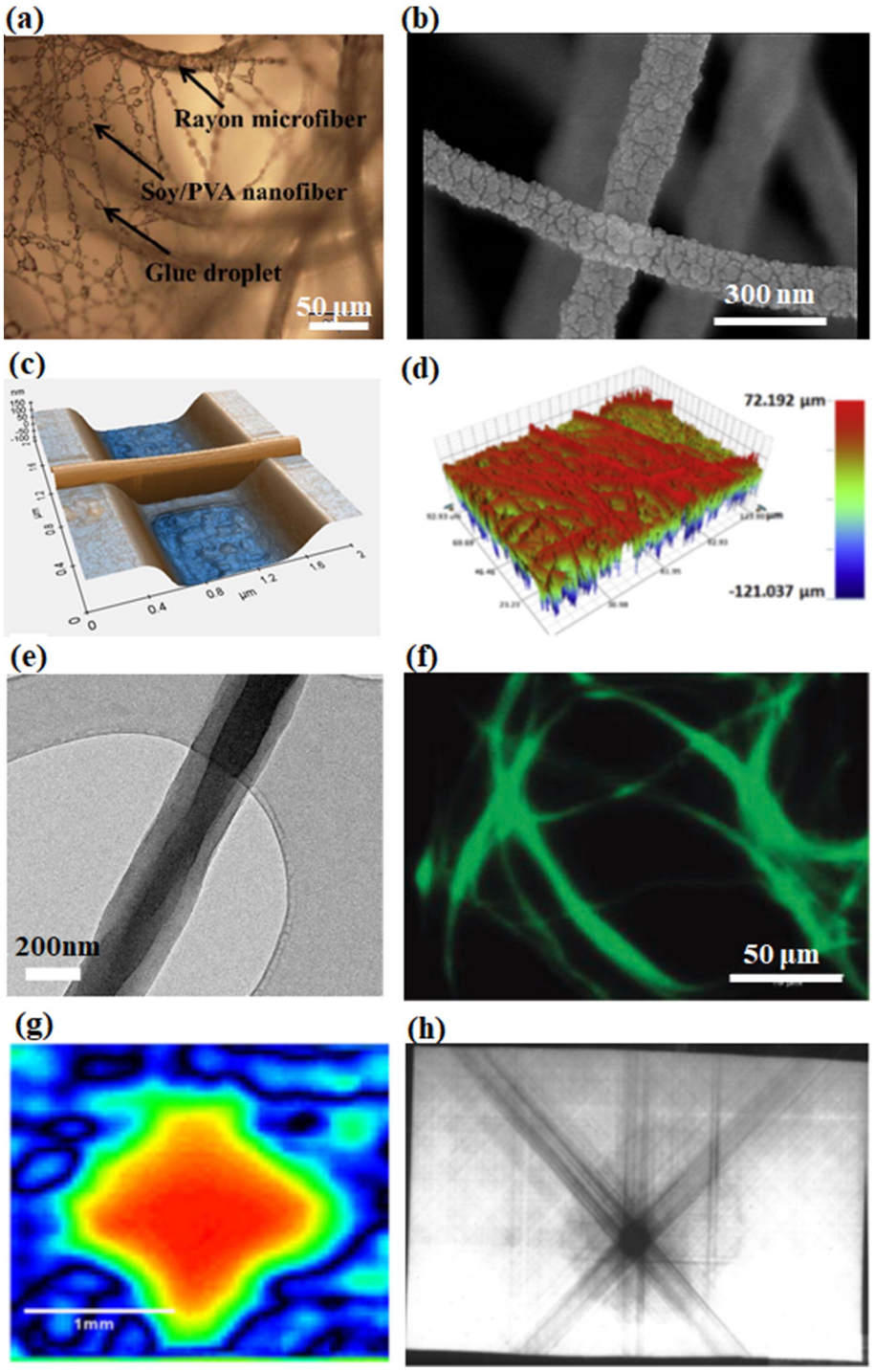

Fig. 16. (a) Optical microscopy image of as-deposited soy protein/PVA nanofibers on rayon pad. Reprinted with permission from [62]. (b) SEM image of electrospun PAN nanofibers. Reprinted with permission from [63]. (c) AFM landscape-mode image of nylon-6 fiber deposited over trench. Reprinted with permission from [64]. (d) Optical profilometry image. Reprinted with permission from [65]. (e) TEM image of resin(core)-PAN(shell) nanofiber. Reprinted with permission from [11]. (f) Fluorescence image of fibers of nylon-6/soy protein blend. Reprinted with permission from [66]. (g) Ultrasonic C-scanning image after impact damage at 0.8 J (i.e., indentation@1400 N). Reprinted with permission from [68]. (h) X-radiograph of quasi-isotropic hollow glass/fiber composite after impact testing obtained using opaque X-ray dye incorporated within impact region. Reprinted with permission from [26].

to measure the energy of adhesion of self-healing mats with respect to various substrates [97,98]. It is a highly reproducible and reliable method that eliminates any edge effects that might occur during delamination [99,100]. Core-shell fiber mats containing an epoxy within the core were cut into pieces and placed on a substrate with a hole in the middle (Fig. 24a). First, the nanofiber mats were made to adhere to the substrates by rolling a metal roller over them [101,102]. In [10], a shaft with a tip 0.5 mm in diameter was inserted through the substrate hole, and the delamination of the adhering nanofiber mat from the substrate was observed. The height, ζ_0, and radius, a, of the emerging delamination blister were measured for different pushing force, P, values. For the axi-symmetric blister test, the energy is given by [10]

$$P\mathrm{d}\zeta_0 = \mathrm{d}U_{\mathrm{elastic}} + T2\pi a\mathrm{d}a \tag{4}$$

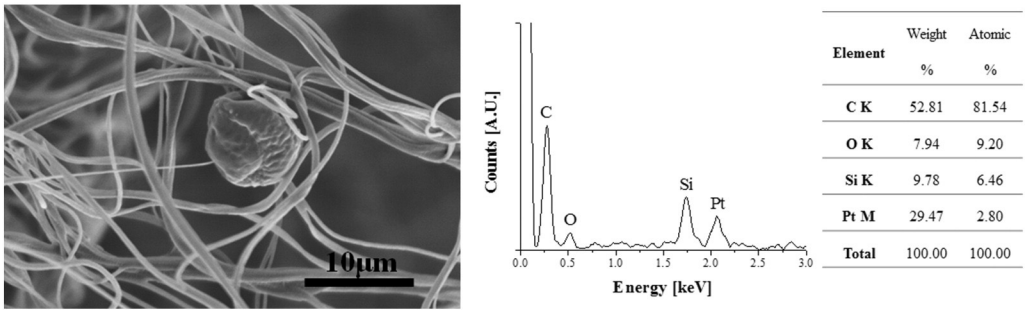

Element	Weight %	Atomic %
C K	52.81	81.54
O K	7.94	9.20
Si K	9.78	6.46
Pt M	29.47	2.80
Total	100.00	100.00

Fig. 17. SEM image of spherical mass (PDMS) released from damaged nanofibers and results of EDX analysis of same. Reprinted with permission from [9].

$$T = \frac{3}{8}\left(\frac{1}{\pi^4 Eh}\right)^{1/3}\left(\frac{P}{a}\right)^{4/3} \quad (5)$$

where $U_{elastic}$ is the elastic energy stored in the test sample (nanofiber mat), E is the Young's modulus of the mat, and h is the thickness of the mat. The Young's modulus, E, values of the fiber mats were determined through a tensile test, whereas the adhesion energy, T, was measured by the blister test using Eq. (5).

The cohesion of two nanofiber mats to each other can also be measured, when one nanofiber mat is fixed to the substrate, and the other one is pressed on it. As the core-shell nanofibers rupture under the pressing action (during the preceding blister test, which measures either the adhesion or cohesion energy), the healing material is released

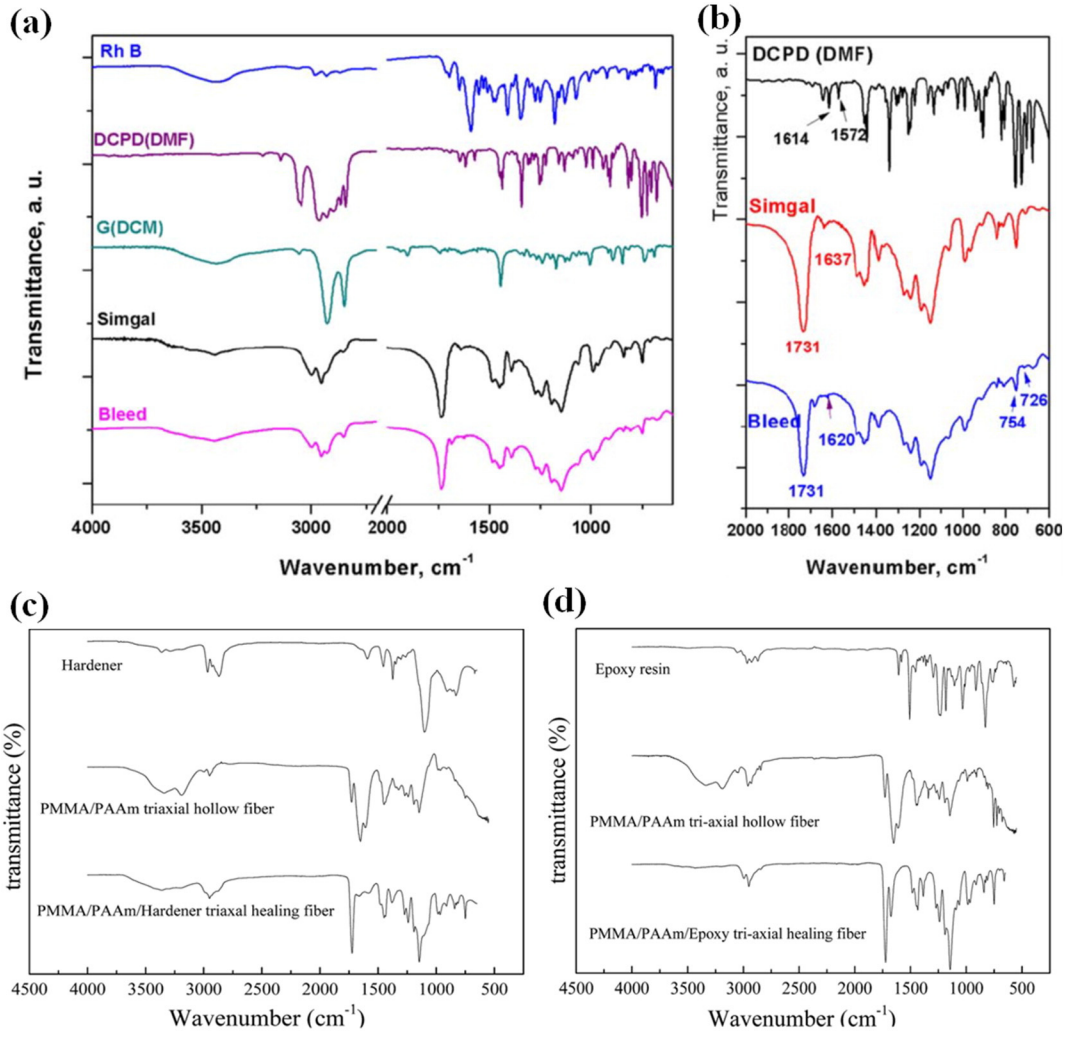

Fig. 18. (a) FTIR spectra of initial materials and self-healing bleed. RhB-Rhodamine B; DCPD (DMF)—10 wt% DCPD solution in DMF; G (DCM)—1 wt% Grubbs' solution in DCM; poly(DCPD) (RhB)—ROMP polymer DCPD with RhB. (b) Spectra of DCPD (DMF), Simgal, and the bleed. Reprinted with permission from [29]. (c) FTIR spectra of hardener, PMMA/PAAm triaxial hollow fibers, and PMMA/PAAm/hardener triaxial fibers. (d) FTIR spectra of epoxy resin, PMMA/PAAm triaxial hollow fibers, and PMMA/PAAm/epoxy triaxial fibers. Reprinted with permission from [19].

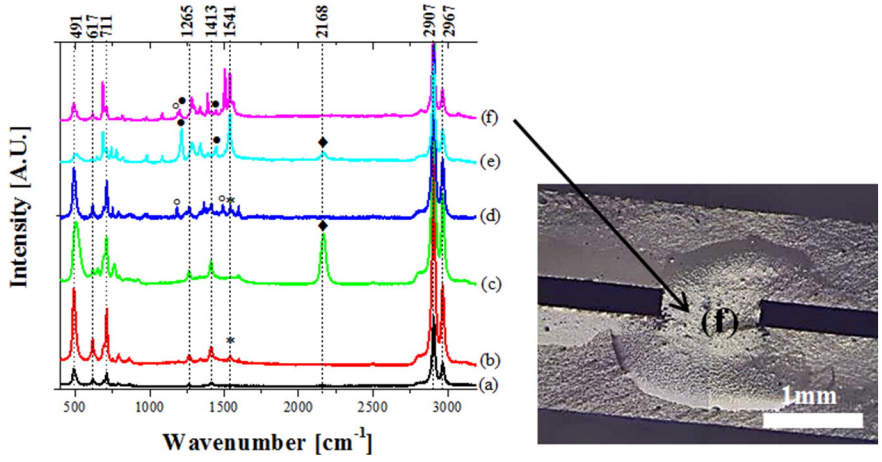

Fig. 19. Raman spectra: (a) cured PDMS, (b) pure resin (⋆), (c) pure curing agent (♦), (d) dyed resin (○), (e) dyed curing agent (●), and (f) mixing zone (optical profilometry image is shown in right-hand side panel). Reprinted with permission from [71].

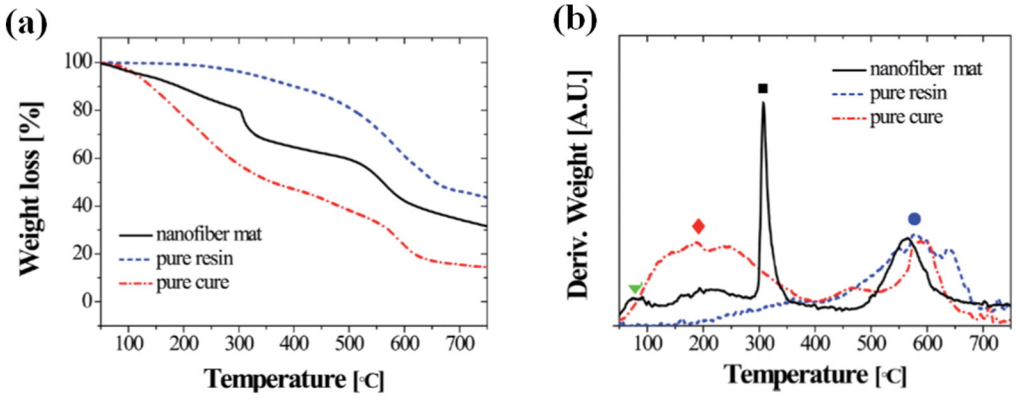

Fig. 20. Thermal analysis of core-shell nanofibers. (a) TGA curves of core materials (PDMS resin and curing agent) and nanofiber mat containing these materials within the cores. (b) DTG curves. Reprinted with permission from [5].

from the core, resulting in polymerization/adhesion between the lower mat and the substrate or between the two mats. It can be seen from Fig. 24c that the cohesion energy of a pristine sample (b-1) and that of a sample tested after being fatigued for 3 h (b-2) are similar, while that of a sample tested after being fatigued for 3 h and subsequently rested for 24 h (b-3) is eight times higher (see Table 1). This suggests that the epoxy precursors released by the damage caused by fatigue have sufficient time to react and cure the damaged interface. This is compelling evidence that the epoxy released from the fiber cores has solidified and reinforced the damaged interface to a significant degree instead of merely healing it (see Fig. 24c).

The results of these studies on the recovery of self-healing materials after mechanical damage are summarized in Table 2. Over the last 16 years, different types of self-healing composites based on vascular

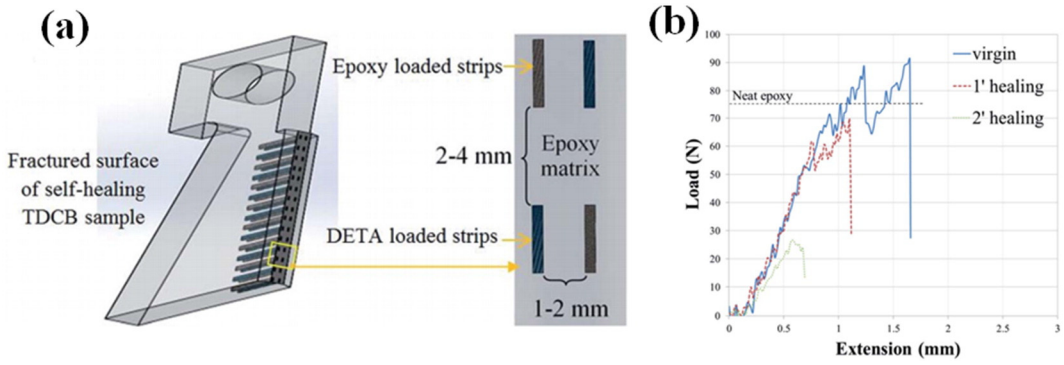

Fig. 21. (a) Schematic illustration of fractured surface and spatial distribution of tapered double-cantilever beam (TDCB) specimens. (b) Typical load-displacement curves for virgin and healed TDCB specimens at 50 °C. Reprinted with permission from [33].

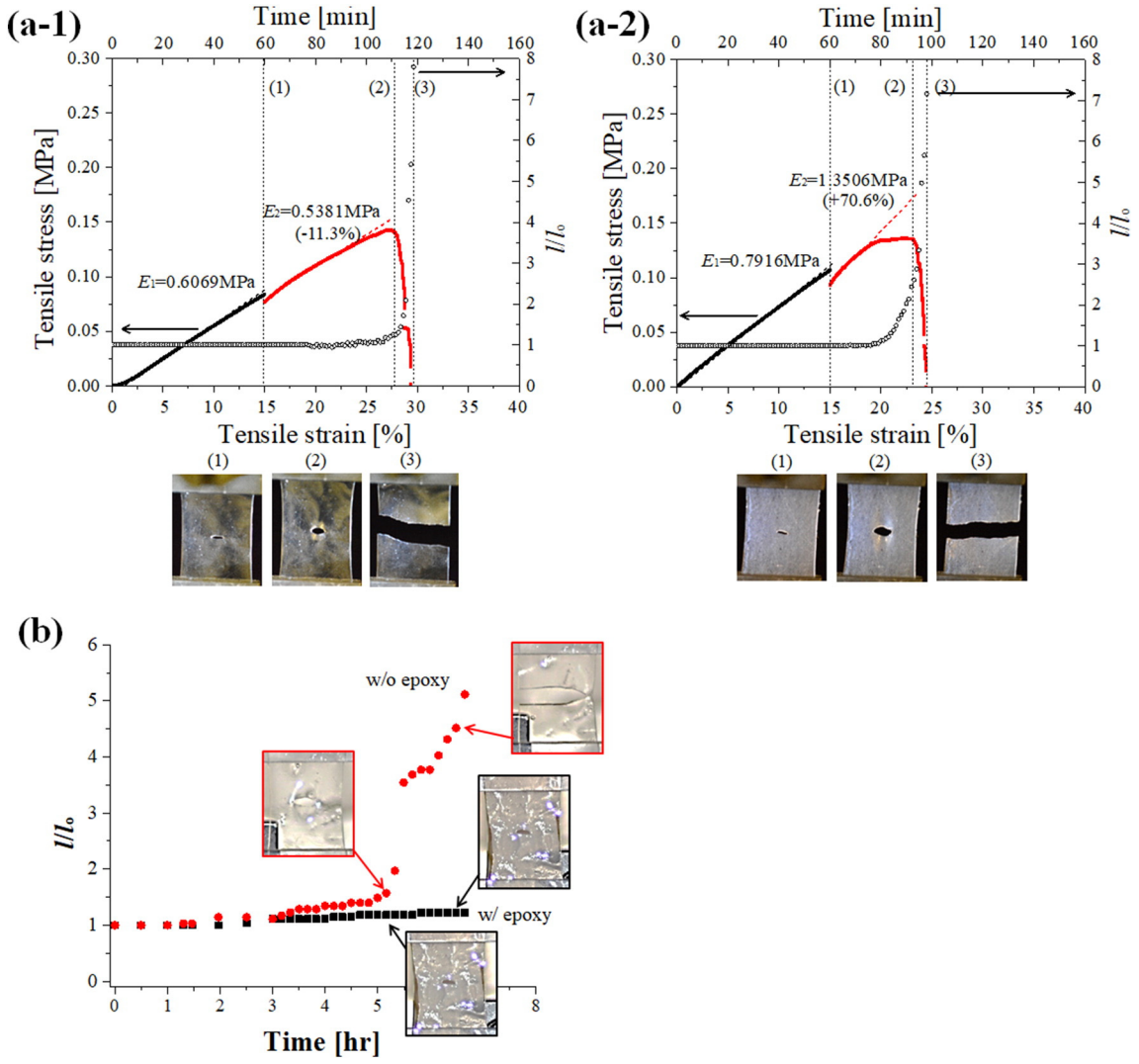

Fig. 22. (a) Stress-strain curves and normalized crack lengths (l/l_o) as determined during tensile tests performed on composites without and with self-healing agents encapsulated within embedded core-shell nanofibers; strain rate of 3 mm/h (= 0.05 mm/min), stretching length of 3 mm; and intermediate holding period of 2 h (after 60 min of stretching). Panel a-1 corresponds to samples with PVDF/PEO fibers alone while panel a-2 corresponds to samples containing nanofibers with epoxy components (healing agent). Black and red bold lines correspond to initial and post-holding stretching stages, respectively. Black open circles show dimensionless crack length as function of time. Reprinted with permission from [60]. (b) Results of static fatigue test performed under fixed strain. Data shown are for composite samples consisting of PDMS matrix embedded with fibers without healing agent, epoxy resin, and hardener (●) and with epoxy resin and hardener (■). Thickness of both samples (without and with epoxy) is 0.60 mm. The strain, ε, applied in both cases is 17.5%. Thicknesses of solution-blown fiber mats (both without and with epoxy) before being encased within PDMS matrix were 0.03–0.04 mm. Reprinted with permission from [59].

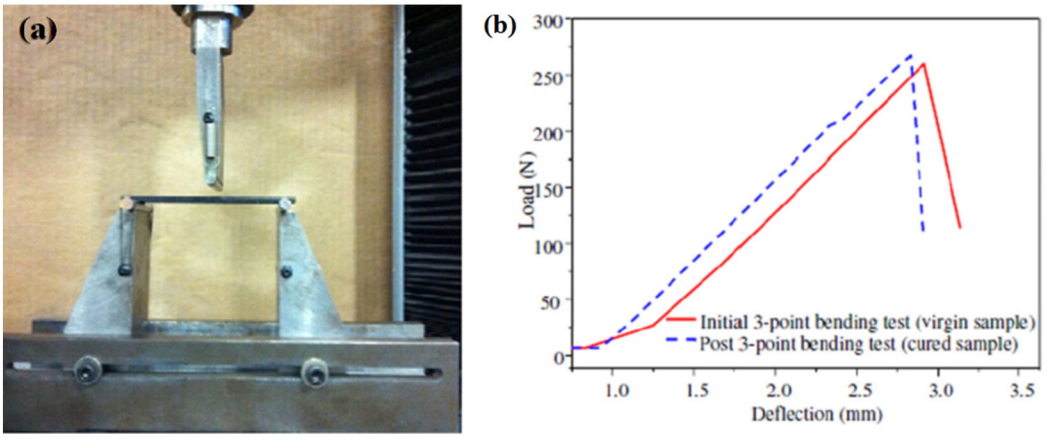

Fig. 23. (a) Three-point bending test setup (span is 75 mm). (b) Comparative load-displacement curves of two typical hybrid multiscale self-healing PMC specimens subjected to three-point bending loads. Reprinted with permission from [7].

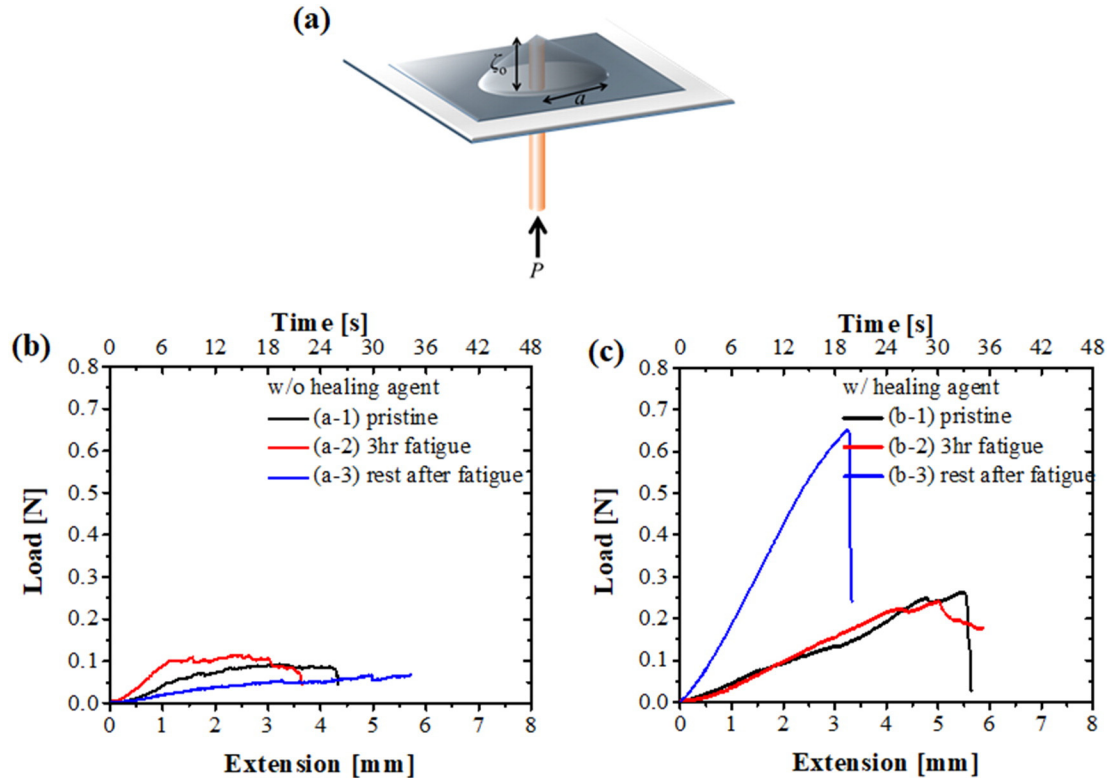

Fig. 24. (a) Schematic of blister test. Reprinted with permission from [10]. (b) Load-extension curves used to determine energy of cohesion between two nanofiber mats without healing agent and (c) with epoxy precursors (healing agent) present in nanofiber cores. Samples were roller-pressed. Curves marked as (−1) correspond to pristine samples, those marked as (−2) are for samples fatigued for 3 h and tested almost immediately after, and those marked as (−3) are for samples fatigued for 3 h, rested for 24 h, and then tested. Reprinted with permission from [24].

systems consisting of hollow fibers, tubing, wires, and fibers have been fabricated and their healing efficiency has been evaluated. Various test techniques such as the tensile test, bending and compression tests, and the blister test have been employed to analyze these composites. In most of these studies, two-part epoxies were used as the healing agent, whose fracture toughness, flexural strength, crack propagation, and adhesion/cohesion energy values were measures of successful healing.

6. Future directions and concluding remarks

Mimicking natural vascular systems in engineering materials is achievable by using core-shell nanofibers whose cores are filled with a self-healing agent. This configuration is beneficial for the following reasons: (i) distributed versus localized (as in the case of microcapsules containing the healing agent) and (ii) nanometer scale instead of micrometer scale (as in the case of microcapsules)—the former can fit the ply areas and does not usually weaken the surrounding matrix. Another benefit of nanofiber-based self-healing systems is that the dispersion of only one of the components needed for the self-healing reaction in the surrounding matrix can be prevented. For this, the self-healing system should consist of two types of nanofibers interwoven such that two different healing agents are present within the core, namely, a resin and its curing agent or an epoxy and its hardener. When released from the damaged core-shell nanofibers, these components react with each other and form solidified stitches that connect the crack banks. As a result, the stiffness and self-cohesion of the damaged material is restored. However, the prevention of delamination and the restoration of adhesion to an "alien" surface remain issues to be resolved and will require additional efforts in the future. On the fabrication side, it has been proven that the solution blowing of core-shell nanofibers, in which a healing agent is encapsulated within the core, is a much more effective process than either co-electrospinning or emulsion spinning. However, even though the solution blowing of various polymers and biopolymers has been demonstrated on the industrial scale using commercially available equipment, it remains to be employed for fabricating core-shell nanofibers containing a healing agent within the core. Only when this has been demonstrated will self-healing engineering materials find wider use in engineering practice. It should be noted that electrospun and solution-blown fibers are usually randomly oriented and are deposited in an uneven manner of surfaces. Moreover, it is hard to ensure the continuous and uniform encapsulation of the healing material within core-shell nano/microfibers when using these techniques. This is an additional obstacle to the scaling-up of the fabrication of self-healing materials at the industrial scale while ensuring high quality.

Table 1
Cohesion energy T and all the parameters measured in the blister test.

	a [mm]	ζ_o [mm]	P [N]	h [mm]	E [MPa]	T [J/m^2]
(a-1)	10.31	3.63	0.037	0.09	2.725	0.071
(a-2)	10.06	1.65	0.018			0.028
(a-3)	13.81	1.52	0.019			0.021
(b-1)	1.63	2.52	0.300	0.08	2.125	15.354
(b-2)	1.69	2.87	0.316			15.575
(b-3)	2.06	2.28	0.189			3.735

Acknowledgement

This work was supported by the International Collaboration Program funded by the Agency for Defense Development. This research was also supported by the Technology Development Program to Solve Climate

Table 2
Different studies of mechanical recovery of vascular self-healing materials.

Vascular type	Healing materials	Damage condition	Healing evaluation	Healing efficiency	Year	Ref.
Hollow glass fiber	Two-part epoxy	Impact, compression tests	Compression strength	N/A	2001	[26]
Hollow glass fiber	Two-part epoxy	Indentation, four-point bending test	Flexural strength	97%	2005	[67]
Hollow glass fiber	Two-part epoxy	Indentation, four-point bending test	Flexural strength	93%	2005	[68]
Hollow glass fiber	Two-part epoxy	Indentation, three-point bending test	Flexural strength	87%	2006, 2007	[27,103]
Hollow glass fiber	Two-part epoxy	Impact, four-point bending test	Flexural strength	97%	2007	[104]
PVC tubing	Two-part epoxy	Four-point bending test	Flexural strength	~100%	2007	[30]
Direct write method	DCPD-Grubbs'	Four-point bending test	Fracture toughness	33–70% (7 cycles)	2007	[4]
Molding	Two-part epoxy	Impact test	Impact energy	65%	2007	[105]
Silicone tubing	Two-part epoxy	Impact, edgewise compression tests	Skin compressive strength	115%	2008	[106]
Hollow glass fiber	Two-part epoxy	Impact, four-point bending test	Flexural strength	95%	2009	[107]
Direct write method	DCPD-Grubbs'	Four-point bending test	Fracture toughness	38% (7 cycles)	2009	[108]
Direct write assembly	Two-part epoxy	Four-point bending test	Fracture toughness	89% (23 cycles)	2009	[109]
Direct write assembly	Two-part epoxy	Four-point bending test	Fracture toughness	~50% (30 cycles)	2009	[31]
Direct write assembly	Two-part epoxy	Mode I fracture test	Fracture toughness	86–30% (13 cycles)	2010	[110]
Wire (removed)	Two-part epoxy	Impact, compression test	Compression strength	99%	2011	[111]
Wire (removed)	Two-part epoxy	Impact, compression test	Compression strength	~100%	2011	[112]
Wire (removed)	Two-part epoxy	Mode I/II fracture test	Fracture toughness	260%/180%	2011	[113]
Wire (removed)	Two-part epoxy	Impact, four-point bending, edgewise compression tests	Fracture toughness	39%	2013	[53]
Casting	Shape memory polymer fiber (SMPF)	Tensile test	Fracture toughness	~100% (7 cycles)	2013	[114]
Hollow glass fiber	Two-part epoxy	Impact test	Impact energy	87%	2014	[115]
Hollow glass fiber	Two-part epoxy	Impact, three-point bending test	Flexural strength	178%	2014	[116]
Vaporization of sacrificial components	Two-part epoxy	Tensile, acoustic emissions test	Fracture toughness, acoustic emission	98%	2014	[117]
Vaporization of sacrificial components	Two-part epoxy	Mode I fracture test	Fracture toughness	125%	2014	[32]
Cell (channel) casting	Shape-conforming dynamic gel	Impact test	Impact energy	62%	2014	[118]
Casting	Thermoplastic healing agent	Three-point bending test	Fracture toughness	>50% (10 cycles)	2015	[39]
Co-electrospinning	PDMS	Tensile test	Young's modulus	125–140% (4 cycles)	2015	[9]
Co-electrospinning	PDMS	Blister test	Adhesion energy	110%	2015	[10]
Tri-axial electrospinning	DCPD	Three-point bending test	Fracture toughness	96%	2015	[19]
Coaxial solution blowing	Two-part epoxy	Blister test	Adhesion energy	318%	2016	[24]
Coaxial solution blowing	Two-part epoxy	Tensile test	Crack propagation	N/A	2016	[59]
Coaxial solution blowing	Two-part epoxy	Tensile test	Young's modulus	171%	2016	[60]
Tri-axial electrospinning	Two-part epoxy	Three-point bending, tensile, acoustic emission test	Fracture toughness, acoustic emission clustering patterns	>86–89% (4-9 cycles)	2017	[20]
Co-electrospinning	PDMS	Tensile test	Crack propagation speed	11% (delay)	2017	[12]
Microchannel	PDMS	Tensile test	Crack propagation	N/A	2017	[71]

Changes of NRF-2016M1A2A2936760, NRF-2013M3A6B1078879, and NRF-2017R1A2B4005639. This study was supported by the Korea Institute of Science and Technology (KIST) Institutional Program.

References

[1] White SR, Sottos NR, Geubelle PH, Moore JS, Kessler MR, Sriram SR, et al. Autonomic healing of polymer composites. Nature 2001;409:794–7.
[2] Zhang P, Li G. Advances in healing-on-demand polymers and polymer composites. Prog Polym Sci 2016;57:32–63.
[3] Dry C. Passive tuneable fibers and matrices. Int J Mod Phys B 1992;6:2763–71.
[4] Toohey KS, Sottos NR, Lewis JA, Moore JS, White SR. Self-healing materials with microvascular networks. Nat Mater 2007;6:581–5.
[5] Lee MW, An S, Lee C, Liou M, Yarin AL, Yoon SS. Self-healing transparent core-shell nanofiber coatings for anti-corrosive protection. J Mater Chem A 2014;2:7045–53.
[6] Yarin AL, Pourdeyhimi B, Ramakrishna S. Fundamentals and applications of micro- and nanofibers. Cambridge: Cambridge University Press; 2014.
[7] Wu X-F, Rahman A, Zhou Z, Pelot DD, Sinha-Ray S, Chen B, et al. Electrospinning core-shell nanofibers for interfacial toughening and self-healing of carbon-fiber/epoxy composites. J Appl Polym Sci 2012;129:1383–93.
[8] Sinha-Ray S, Pelot DD, Zhou ZP, Rahman A, Wu X-F, Yarin AL. Encapsulation of self-healing materials by coelectrospinning, emulsion electrospinning, solution blowing and intercalation. J Mater Chem 2012;22:9138–46.
[9] Lee MW, An S, Jo HS, Yoon SS, Yarin AL. Self-healing nanofiber-reinforced polymer composites: 1. Tensile testing and recovery of mechanical properties. ACS Appl Mater Interfaces 2015;7:19546–54.
[10] Lee MW, An S, Jo HS, Yoon SS, Yarin AL. Self-healing nanofiber-reinforced polymer composites: 2. Delamination/debonding, and adhesive and cohesive properties. ACS Appl Mater Interfaces 2015;7:19555–61.
[11] An S, Liou M, Song KY, Jo HS, Lee MW, Al-Deyab SS, et al. Highly flexible transparent self-healing composite based on electrospun core-shell nanofibers produced by co-axial electrospinning for anti-corrosion and electrical insulation. Nanoscale 2015;7:17778–85.
[12] Lee MW, Sett S, An S, Yoon SS, Yarin AL. Self-healing nano-textured vascular-like materials: mode I crack propagation. ACS Appl Mater Interfaces 2017;9:27223–31.
[13] Sun Z, Zussman E, Yarin AL, Wendorff JH, Greiner A. Compound core-shell polymer nanofibers by co-electrospinning. Adv Mater 2003;15:1929–32.
[14] Park J-H, Braun PV. Coaxial electrospinning of self-healing coatings. Adv Mater 2010;22:496–9.
[15] Zanjani JSM, Okan BS, Menceloglu YZ, Yildiz M. Design and fabrication of multi-walled hollow nanofibers by triaxial electrospinning as reinforcing agents in nanocomposites. J Reinf Plast Compos 2015;34:1273–86.
[16] Han D, Steckl AJ. Triaxial electrospun nanofiber membranes for controlled dual release of functional molecules. ACS Appl Mater Interfaces 2013;5:8241–5.
[17] D-G Yu, Li X-Y, Wang X, Yang J-H, Bligh SWA, Williams GR. Nanofibers fabricated using triaxial electrospinning as zero order drug delivery systems. ACS Appl Mater Interfaces 2015;7:18891–7.
[18] Khalf A, Singarapu K, Madihally SV. Influence of solvent characteristics in triaxial electrospun fiber formation. React Funct Polym 2015;90:36–46.
[19] Zanjani JSM, Okan BS, Letofsky-Papst I, Menceloglu Y, Yildiz M. Repeated self-healing of nano and micro scale cracks in epoxy based composites by tri-axial electrospun fibers including different healing agents. RSC Adv 2015;5:73133–45.
[20] Zanjani JSM, Okan BS, Yilmaz C, Menceloglu Y, Yildiz M. Monitoring the Interface and bulk self-healing capability of triaxial electrospun fibers in glass fiber reinforced epoxy composites. Composites A 2017;99:221–32.
[21] Yarin AL. Coaxial electrospinning and emulsion electrospinning of core–shell fibers. Polym Adv Technol 2011;22:310–7.
[22] Sinha-Ray S, Yarin AL, Pourdeyhimi B. The production of 100/400 nm inner/outer diameter carbon tubes by solution blowing and carbonization of core-shell nanofibers. Carbon 2010;48:3575–8.
[23] Shi L, Zhuang X, Tao X, Cheng B, Kang W. Solution blowing nylon 6 nanofiber mats for air filtration. Fibers Polym 2013;14:1485–90.
[24] Lee MW, Yoon SS, Yarin AL. Solution-blown core—shell self-healing nano- and microfibers. ACS Appl Mater Interfaces 2016;8:4955–62.
[25] Kolbasov A, Sinha-Ray S, Joijode A, Hassan MA, Brown D, Maze B, et al. Industrial-scale solution blowing of soy protein nanofibers. Ind Eng Chem Res 2016;55:323–33.
[26] Bleay SM, Loader CB, Hawyes VJ, Humberstone L, Curtis PT. A smart repair system for polymer matrix composites. Composites A 2001;32:1767–76.

[27] Trask RS, Bond IP. Biomimetic self-healing of advanced composite structures using hollow glass fibres. SMaS 2006;15:704–10.
[28] Fifo O, Ryan K, Basu B. Glass fibre polyester composite with in vivo vascular channel for use in self-healing. SMaS 2014;23:095017.
[29] Yerro O, Radojevic V, Radovic I, Petrovic M, Uskokovic PS, Stojanovic DB, et al. Thermoplastic acrylic resin with self-healing properties. Polym Eng Sci 2016;56:251–7.
[30] Williams HR, Trask RS, Bond IP. Self-healing composite sandwich structures. SMaS 2007;16:1198–207.
[31] Hansen CJ, Wu W, Toohey KS, Sottos NR, White SR, Lewis JA. Self-healing materials with interpenetrating microvascular networks. Adv Mater 2009;21:4143–7.
[32] Patrick JF, Hart KR, Krull BP, Diesendruck CE, Moore JS, White SR, et al. Continuous self-healing life cycle in vascularized structural composites. Adv Mater 2014;26:4302–8.
[33] Vahedi V, Pasbakhsh P, Piao CS, Seng CEA. Facile method for preparation of self-healing epoxy composites: using electrospun nanofibers as microchannels. J Mater Chem A 2015;3:16005–12.
[34] Li G, John MA. Self-healing smart syntactic foam under multiple impacts. Compos Sci Technol 2008;68:3337–43.
[35] Li G, Uppu N. Shape memory polymer based self-healing syntactic foam: 3-D confined thermomechanical characterization. Compos Sci Technol 2010;70:1419–27.
[36] Li G, Nettles D. Thermomechanical characterization of a shape memory polymer based self-repairing syntactic foam. Polymer 2010;51:755–62.
[37] Zhang P, Ogunmekan B, Ibekwe S, Jerro D, Pang S-S, Li G. Healing of shape memory polyurethane fiber-reinforced syntactic foam subjected to tensile stress. J Intell Mater Syst Struct 2016;27:1792–801.
[38] Champagne J, Pang S-S, Li G. Effect of confinement level and local heating on healing efficiency of self-healing particulate composites. Compos Part B 2016;97:344–52.
[39] Zhang P, Li G. Healing-on-demand composites based on polymer artificial muscle. Polymer 2015;64:29–38.
[40] Brown EN, White SR, Sottos NR. Microcapsule induced toughening in a self-healing polymer composite. J Mater Sci 2004;39:1703–10.
[41] Mauldin TC, Rule JD, Sottos NR, White SR, Moore JS. Self-healing kinetics and the stereoisomers of dicyclopentadiene. J R Soc Interface 2007;4:389–93.
[42] van der Zwaag S. Self healing materials: an alternative approach to 20 centuries of materials science. Heidelberg: Springer; 2007.
[43] Perring M, Long TR, Bowden NB. Epoxidation of the surface of polydicyclopentadiene for the self-assembly of organic monolayers. J Mater Chem 2010;20:8679–85.
[44] Lenhardt JM, Kim SH, Nelson AJ, Singhal P, Baumann Jr TF, Satcher JH. Increasing the oxidative stability of poly(dicyclopentadiene) aerogels by hydrogenation. Polymer 2013;54:542–7.
[45] Keller MW, White SR, Sottos NRA. Self-healing poly(dimethyl siloxane) elastomer. Adv Mater 2007;17:2399–404.
[46] Cho SH, Andersson HM, White SR, Sottos NR, Braun PV. Polydimethylsiloxane-based self-healing materials. Adv Mater 2006;18:997–1000.
[47] Lee MW, An S, Lee C, Liou M, Yarin AL, Yoon SS. Hybrid self-healing matrix using core−shell nanofibers and capsuleless microdroplets. ACS Appl Mater Interfaces 2014;6:10461–8.
[48] Lee MW, An S, Kim Y-I, Yoon SS, Yarin AL. Self-healing three-dimensional bulk materials based on core-shell nanofibers. Chem Eng J 2018;334:1093–100.
[49] Neisiany RE, Khorasani SN, Lee JKY, Ramakrishna S. Encapsulation of epoxy and amine curing agent in PAN nanofibers by coaxial electrospinning for selfhealing purposes. RSC Adv 2016;6:70056–63.
[50] Campbell DJ, Beckman KJ, Calderon CE, Doolan PW, Ottosen RM, Ellis AB, et al. Replication and compression of bulk and surface structures with polydimethylsiloxane elastomer. J Chem Educ 1999;75:537–41.
[51] Goosey MT. Epoxide resins and their formulation. In: Goosey MT, editor. Plastics for electronics. Dordrecht: Springer Netherlands; 1985. p. 99–136.
[52] Raquez J-M, Deleglisea M, Lacrampea M-F, Krawczak P. Thermosetting (bio)materials derived from renewable resources: a critical review. Prog Polym Sci 2010;35:487–509.
[53] Chen C, Peters K, Li Y. Self-healing sandwich structures incorporating an interfacial layer with vascular network. SMaS 2013;22:025031.
[54] Jones AR, Watkins CA, White SR, Sottos NR. Self-healing thermoplastic-toughened epoxy. Polymer 2015;74:254–61.
[55] Blaiszik BJ, Caruso MM, McIlroy DA, Moore JS, White SR, Sottos NR. Microcapsules filled with reactive solutions for self-healing materials. Polymer 2009;50:990–7.
[56] Garcia FG, Soares BG, Pita VJRR, Sanchez R, Rieumont J. Mechanical properties of epoxy networks based onDGEBA and aliphatic amines. J Appl Polym Sci 2007;106:2047–55.
[57] Denq BL, Hu YS, Chen LW, Chiu WY, Wu TR. The curing reaction and physical properties of DGEBA/DETA epoxy resin blended with propyl ester phosphazene. J Appl Polym Sci 1999;74:229–37.
[58] Flint S, Markle T, Thompson S, Wallace E, Bisphenol A. Exposure, effects, and policy: a wildlife perspective. J Environ Manag 2012;104:19–34.
[59] Lee MW, Sett S, Yoon SS, Yarin AL. Fatigue of self-healing nanofiber-based composites: static test and subcritical crack propagation. ACS Appl Mater Interfaces 2016;8:18462–70.
[60] Lee MW, Sett S, Yoon SS, Yarin AL. Self-healing of nanofiber-based composites in the course of stretching. Polymer 2016;103:180–8.
[61] Farquharson S, Smith W, Rose J, Shaw M. Correlations between molecular (Raman) and macroscopic (rheology) data for process monitoring of thermoset composite. Journal of Process Analytical Chemistry 2002;7:45.
[62] Sett S, Lee MW, Weith M, Pourdeyhimi B, Yarin AL. Biodegradable and biocompatible soy protein/polymer/adhesive sticky nano-textured interfacial membranes for prevention of esca fungi invasion into pruning cuts and wounds of vines. J Mater Chem B 2015;3:2147–62.
[63] An S, Joshi BN, Lee MW, Kim NY, Yoon SS. Electrospun graphene-ZnO nanofiber mats for photocatalysis applications. Appl Surf Sci 2014;294:24–8.
[64] Sinha-Ray S, Lee MW, Sinha-Ray S, An S, Pourdeyhimi B, Yoon SS, et al. Supersonic nanoblowing: a new ultra-stiff phase of nylon 6 in 20–50 nm confinement. J Mater Chem C 2012;1:3491–8.
[65] Ghosal A, Sinha-Ray S, Sinha-Ray S, Yarin AL, Pourdeyhimi B. Numerical modeling and experimental study of solution-blown nonwovens formed on a rotating drum. Polymer 2016;105:255–63.
[66] Sinha-Ray S, Zhang Y, Yarin AL, Davis S, Pourdeyhimi B. Solution blowing of soy protein fibers. Biomacromolecules 2011;12:2357–63.
[67] Pang JWC, Bond IP. 'Bleeding composites'—damage detection and self-repair using a biomimetic approach. Composites A 2005;36:183–8.
[68] Pang JWC, Bond IPA. Hollow fibre reinforced polymer composite encompassing self-healing and enhanced damage visibility. Compos Sci Technol 2005;65:1791–9.
[69] Jayes L, Hard AP, Sene C, Parker SF, Jayasooriya UA. Vibrational spectroscopic analysis of silicones: a Fourier transform-Raman and inelastic neutron scattering investigation. Anal Chem 2003;75:742–6.
[70] Colthup NB, Daly LH, Wiberley SE. Introduction to infrared and Raman spectroscopy. Third Edition. New York: Academic Press; 1975.
[71] Lee MW, Yoon SS, Yarin AL. Release of self-healing agents in a material: what happens next? ACS Appl Mater Interfaces 2017;9:17449–55.
[72] Merad L, Cochez M, Margueron S, Jauchem F, Ferriol M, Benyoucef B, et al. In-situ monitoring of the curing of epoxy resins by Raman spectroscopy. Polym Test 2009;28:42–5.
[73] Maiti NC, Apetri MM, Zagorski MG, Carey PR, Anderson VE. Raman spectroscopic characterization of secondary structure in natively unfolded proteins: α-synuclein. J Am Chem Soc 2004;126:2399–408.
[74] Mostovoy S, Crosley PB, Ripling EJ. Use of crack-line-loaded specimens for measuring planestrain fracture toughness. J Mater 1967;2:661–81.
[75] Jin H, Miller GM, Sottos NR, White SR. Fracture and fatigue response of a self-healing epoxy adhesive. Polymer 2011;52:1628–34.
[76] Hart KR, Sottos NR, White SR. Repeatable self-healing of an epoxy matrix using imidazole initiated polymerization. Polymer 2015;67:174–84.
[77] Jones AS, Rule JD, Moore JS, Sottos NR, White SR. Life extension of self-healing polymers with rapidly growing fatigue cracks. J R Soc Interface 2007;4:395–403.
[78] Kessler MR, Sottos NR, White SR. Self-healing structural composite materials. Compos Part A 2003;34:743–53.
[79] Brown EN, White SR, Sottos NR. Retardation and repair of fatigue cracks in a microcapsule toughened epoxy composite – part I: manual infiltration. Compos Sci Technol 2005;65:2466–73.
[80] Brown EN. Use of the tapered double-cantilever beam geometry for fracture toughness measurements and its application to the quantification of self-healing. JStA 2011;46:167–86.
[81] Rule JD, Brown EN, Sottos NR, White SR, Moore JS. Wax-protected catalyst microspheres for efficient self-healing materials. Adv Mater 2005;17:205–8.
[82] Brown EN, Sottos NR, White SR. Fracture testing of a self-healing polymer composite. ExM 2002;42:372–9.
[83] Rule JD, Sottos NR, White SR. Effect of microcapsule size on the performance of self-healing polymers. Polymer 2007;48:3520–9.
[84] Irwin GR, Kies JA. Critical energy rate analysis of fracture strength. American Welding Society Journal 1954;33:193–8.
[85] Khansari S, Sinha-Ray S, Yarin AL, Pourdeyhimi B. Stress-strain dependence for soy-protein nanofiber mats. J Appl Phys 2012;111:044906.
[86] Sinha-Ray S, Khansari S, Yarin AL, Pourdeyhimi B. Effect of chemical and physical cross-linking on tensile characteristics of solution-blown soy protein nanofiber mats. Ind Eng Chem Res 2012;51:15109–21.
[87] Khansari S, Sinha-Ray S, Yarin AL, Pourdeyhimi B. Biopolymer-based nanofiber mats and their mechanical characterization. Ind Eng Chem Res 2013;52:15104–13.
[88] Sinha-Ray S, Yarin AL, Pourdeyhimi B. Meltblown fiber mats and their tensile strength. Polymer 2014;55:4241–7.
[89] Stafford GD, Smith DC. Some studies of the properties of denture base polymers. Br Dent J 1968;125:337–42.
[90] Stafford GD, Handley RW. Transverse bend testing of denture base polymers. J Dent 1975;3:251–5.
[91] Whitney J, Browning C, Mair A. Analysis of the flexure test for laminated composite materials. ASTM International: West Conshohocken, PA; 1974.
[92] Standard Methods of Test for Flexural Properties of Plastics. ASTM: D790-71: American Society for Testing and Materials; 1970.
[93] Standard Test Method for Flexural Properties of Unreinforced and Reinforced Plastics and Electrical Insulating Materials by Four-Point Bending. D6272: American Society for Testing and Materials; 1998.
[94] Papa E, Corigliano A. Mechanical behaviour of a syntactic foam/glass fibre composite sandwich: experimental results. Struct Eng Mech 2001;12:169–88.
[95] Li AAW. An experimental investigation on the three-point bending behavior of composite laminate IOP Conference series. Mater Sci Eng 2014;62:012016.
[96] Laffan MJ, Pinho ST, Robinson P, McMillan AJ. Translaminar fracture toughness testing of composites: a review. Polym Test 2012;31:481–9.
[97] Malyshev BM, Salganik RL. The strength of adhesive joints using the theory of cracks. Int J Fract Mech 1965;1:114–28.
[98] Wan K-T, Mai Y-W. Fracture mechanics of a shaft-loaded blister of thin flexible membrane on rigid substrate. IJFr 1995;74:181–97.
[99] Obreimoff JW. The splitting strength of mica. Proc R Soc Lond A 1930;127:290–7.

[100] Hutchinson JW, Suo Z. Mixed mode cracking in layered materials. Adv Appl Mech 1992;29:63–191.
[101] Na H, Chen P, Wan K-T, Wong S-C, Li Q, Ma Z. Measurement of adhesion work of electrospun polymer membrane by shaft-loaded blister test. Langmuir 2012;28:6677–83.
[102] Wong S-C, Na H, Chen P. Measurement of adhesion energy of electrospun polymer membranes using a shaft-loaded blister test. 13th International Conference on Fracture; 2013 Beijing, China.
[103] Trask RS, Williams GJ, Bond IP. Bioinspired self-healing of advanced composite structures using hollow glass fibres. J R Soc Interface 2007;4:363–71.
[104] Williams G, Trask R, Bond I. A self-healing carbon fibre reinforced polymer for aerospace applications. Compos Part A 2007;38:1525–32.
[105] Hayes SA, Zhang W, Branthwaite M, Jones FR. Self-healing of damage in fibre-reinforced polymer-matrix composites. J R Soc Interface 2007;4:381–7.
[106] Williams HR, Trask RS, Bond IP. Self-healing sandwich panels: restoration of compressive strength after impact. Compos Sci Technol 2008;68:3171–7.
[107] Williams GJ, Bond IP, Trask RS. Compression after impact assessment of self-healing CFRP. Composites A 2009;40:1399–406.
[108] Toohey KS, Sottos NR, White SR. Characterization of microvascular-based self-healing coatings. ExM 2009;49:707–17.
[109] Toohey KS, Hansen CJ, Lewis JA, White SR, Sottos NR. Delivery of two-part self-healing chemistry via microvascular networks. Adv Mater 2009;19:1399–405.
[110] Hamilton AR, Sottos NR, White SR. Self-healing of internal damage in synthetic vascular materials. Adv Mater 2010;22:5159–63.
[111] Norris CJ, Meadway GJ, O'Sullivan MJ, Bond IP, Trask RS. Self-healing fibre reinforced composites via a bioinspired vasculature. Adv Funct Mater 2011;21:3624–33.
[112] Norris CJ, Bond IP, Trask RS. The role of embedded bioinspired vasculature on damage formation in self-healing carbon fibre reinforced composites. Composites A 2011;42:639–48.
[113] Norris CJ, Bond IP, Trask RS. Interactions between propagating cracks and bioinspired self-healing vascules embedded in glass fibre reinforced composites. Compos Sci Technol 2011;71:847–53.
[114] Li G, Ajisafe O, Meng H. Effect of strain hardening of shape memory polymer fibers on healing efficiency of thermosetting polymer composites. Polymer 2013;54:920–8.
[115] Zainuddin S, Arefinb T, Fahim A, Hosur MV, Tyson JD, Kumar A, et al. Recovery and improvement in low-velocity impact properties of e-glass/epoxy composites through novel self-healing technique. Compos Struct 2014;108:277–86.
[116] Kling S, Czigany T. Damage detection and self-repair in hollow glass fiber fabric-reinforced epoxy composites via fiber filling. Compos Sci Technol 2014;99:82–8.
[117] Coppola AM, Thakre PR, Sottos NR, White SR. Tensile properties and damage evolution in vascular 3D woven glass/epoxy composites. Composites A 2014;59:9–17.
[118] White SR, Moore JS, Sottos NR, Krull BP, Cruz WAS, Gergely RCR. Restoration of large damage volumes in polymers. Science 2014;344:620–3.